The Astrophysical Journal, 870:105 (9pp), 2019 January 10 https://doi.org/10.3847/1538-4357/aaf1c5

Analysis of the Duration–Hardness Ratio Plane of Gamma-Ray Bursts Using Skewed Distributions

Mariusz Tarnopolski
Astronomical Observatory, Jagiellonian University, Orla 171, 30–244, Kraków, Poland; mariusz.tarnopolski@uj.edu.pl
Received 2018 August 20; revised 2018 November 2; accepted 2018 November 15; published 2019 January 14

Abstract

The two widely accepted classes of gamma-ray bursts (GRBs), short and long, are with confidence ascribed to mergers of compact objects and collapse of massive stars, respectively. A third, intermediate/soft class, remains putative. Its existence was claimed based on univariate and bivariate analyses of GRB observables modeled with Gaussian distributions. This, however, may not be the appropriate approach, as it has already been shown that the univariate distributions of durations are better described by mixtures of two skewed components rather than three Gaussian ones. This paper investigates whether data in the duration–hardness ratio plane is better modeled by mixtures of skewed bivariate distributions than by normal ones. The archival data set of the *Compton Gamma-Ray Observatory*/BATSE and *Fermi*/Gamma-ray Burst Monitor data from the most recent catalog release are examined. The preferred model is chosen based on two information criteria, Akaike and Bayesian. It is found that the best description is given by a two-component mixture of skewed Student-*t* distributions, which outperforms any other model considered. This implies that the distribution of the studied parameters is intrinsically skewed, introducing spurious Gaussian components, and hence the third class is unlikely to be a real phenomenon. Its existence, based on statistical inference, is therefore rejected as unnecessary to explain the observations.

Key words: gamma-ray burst: general – methods: data analysis – methods: statistical

1. Introduction

Gamma-ray bursts (GRBs, Klebesadel et al. 1973) were early recognized to have a bimodal duration distribution (Mazets et al. 1981). The division between short (Eichler et al. 1989; Paczynski 1991; Narayan et al. 1992) and long GRBs (Woosley 1993; Paczyński 1998; MacFadyen & Woosley 1999) was established, based on the distribution of T_{90} (the time during which 90% of the GRB's fluence is accumulated, starting from the time at which 5% of the total fluence is detected), to be at $T_{90} \simeq 2$ s (Kouveliotou et al. 1993; but see also Fynbo et al. 2006; King et al. 2007; Kann et al. 2011; Bromberg et al. 2013; Tarnopolski 2015a, 2015b; Li et al. 2016). The progenitors of short GRBs are believed to be double neutron star (NS–NS) or NS-black hole (BH) mergers (Nakar 2007). The association of a kilonova with GRB 130603B provided strong evidence for the nature of the progenitors of short GRBs (Tanvir et al. 2013). The recent detection of the gravitational wave event together with a short GRB as its electromagnetic counterpart, GW/GRB 170817, further confirmed the relation between short GRBs and compact-object mergers (Abbott et al. 2017a, 2017b; Goldstein et al. 2017; Savchenko et al. 2017). The progenitors of long GRBs are associated with supernovae Ic (Filippenko 1997) related with collapse of massive, e.g., Wolf–Rayet or blue supergiant, stars (Galama et al. 1998; Hjorth et al. 2003; Stanek et al. 2003; Woosley & Bloom 2006; Cano et al. 2017; Perna et al. 2018). No connection between short GRBs and supernovae has been proven (Zhang et al. 2009; Ruffini et al. 2016).

The durations T_{90} were noticed early on (McBreen et al. 1994; Koshut et al. 1996; Kouveliotou et al. 1996) to roughly follow a lognormal distribution (i.e., $\log T_{90}$ to be normal), and routinely fitted thereafter as such. Horváth (1998) found a prominent third peak, between the short and long groups, in the $\log T_{90}$ distribution of GRBs detected by the Burst And Transient Explorer on board the *Compton Gamma-Ray Observatory* (*CGRO*/BATSE; Meegan et al. 1992; Paciesas et al. 1999), and hence claimed the existence of an intermediate-duration class of GRBs. However, when more data was accumulated, this peak blended into the bulk of the distribution, manifesting itself only as a small bump on the shorter side of the long GRBs group (Horváth 2002; Tarnopolski 2015c), adding to the skewness of the component. The evidence for a third normal component in $\log T_{90}$ was found also in *Swift* Burst Alert Telescope data (Horváth et al. 2008, 2010; Zhang & Choi 2008; Huja et al. 2009; Zitouni et al. 2015; Zhang et al. 2016). *Swift* GRBs form the largest sample of GRBs with measured redshifts observed by the same instrument, making the analysis in both observer and rest frames possible. It was found (Huja et al. 2009; Tarnopolski 2016a; Zhang et al. 2016; Kulkarni & Desai 2017) that three and two Gaussian components are required in the observer and rest frames, respectively; however, Zitouni et al. (2015) found three groups in both frames. Interestingly, only two components are required for the BATSE data set in the observer frame (Zitouni et al. 2015; Zhang et al. 2016), contrary to the findings of Horváth (2002). Kulkarni & Desai (2017) also did not find decisive evidence for a third component in the case of BATSE. Regarding *Fermi* Gamma-ray Burst Monitor (GBM, Gruber et al. 2014; von Kienlin et al. 2014; Narayana Bhat et al. 2016), Bystricky et al. (2012), Narayana Bhat et al. (2016), Zhang et al. (2016), and Kulkarni & Desai (2017) found that two components suffice for the logarithmic duration distribution to be adequately described. Using pseudo-redshifts derived from the L_p–E_p relation (Yonetoku et al. 2010; Tsutsui et al. 2013), the same conclusion was reached by Zitouni et al. (2018).

Evidence for a third normal component was found, however, in the *RHESSI* data set (Řípa et al. 2009). In the data from *BeppoSAX* (Frontera et al. 2009), due to low sensitivity to short GRBs (caused by a 1 s short integration time), there were only two peaks in the $\log T_{90}$ distribution, corresponding to intermediate and long classes (Horváth 2009). In case of *Suzaku* Wide-band All-sky Monitor, a two-component mixture of lognormal distributions is favored over a three-component one (Ohmori et al. 2016).

It was argued (Koen & Bere 2012; Tarnopolski 2015c) that the logarithmic duration distribution need not necessarily be normal; the asymmetry (skewness) can originate from, e.g., an asymmetric distribution of the progenitor envelope mass (Zitouni et al. 2015). Therefore, the BATSE, *Swift*, and *Fermi* data sets were examined previously with skewed distributions (Tarnopolski 2016b, 2016c; Kwong & Nadarajah 2018). The reasoning is that modeling an inherently skewed distribution with a mixture of symmetric ones requires excessive components to be included, resulting in a spurious determination of the number of underlying classes (Koen & Bere 2012). It is conceptually and technically easier to introduce an additional parameter in the modeling of short and long GRBs rather than to invent a new physical mechanism giving rise to an elusive intermediate class. It was indeed found that mixtures of two skewed components are either significantly better than, or at least as good as, three-component symmetric models, meaning that the third class is discarded as unnecessary (Tarnopolski 2016b). Moreover, a careful analysis of the properties of the presumed class of intermediate GRBs showed that they differ from long GRBs only in having lower luminosities (de Ugarte Postigo et al. 2011), so that they might be simply a low-luminosity tail of the long GRBs group.

A univariate analysis cannot, however, reveal all the intricacies of separating GRBs into meaningful classes. A natural step is to examine a two-dimensional realm of the T_{90}–H plane composed of the duration and ratio of fluences in two energy bands (i.e., hardness ratio). Mukherjee et al. (1998); Horváth et al. (2006; with BATSE data), Řípa et al. (2009; *RHESSI*), Horváth et al. (2010), Veres et al. (2010; *Swift*) performed analyses of the T_{90}–H distribution similarly to the univariate case, i.e., assumed a bivariate Gaussian mixture model and seeked the number of components that fits the data best; they all found a three-component model to be more favorable than that with two components. Řípa et al. (2012), however, arrived at only two components in the case of the *RHESSI* data set. Horvath et al. (2012) performed a principal component analysis that was followed by fitting mixtures of bivariate Gaussian distribution; it was found that a three-component model is the optimal one in terms of goodness of fit. On the other hand, Yang et al. (2016) examined *Swift* GRBs with measured redshift, and showed that two components suffice in both the observer and rest frames. For the *Fermi* sample, contradictory results have been obtained: Narayana Bhat et al. (2016) arrived at two, while Horváth et al. (2018) at three components as the most favorable.

Several classifications were done in higher-dimensional parameter spaces. Mukherjee et al. (1998) performed nonparametric and multinormal clustering of 797 BATSE 3B GRBs in a space of six parameters (durations T_{90} and T_{50}, defined in a similar fashion as T_{90}, peak flux measured in 256 ms bins P_{256}, total fluence $F_{\rm tot}$, and hardness ratios H_{32} and H_{321}). The nonparametric approach yielded ambiguous results, pointing at two or three clusters, while the multinormal modeling (in a three-dimensional space of T_{90}, total fluence and H_{321}—the hardness ratio H_{32} was eliminated) indicated the GRB population consisted of three classes. It should be emphasized that the examined data set was the same as that in Horváth (1998), where a prominent third peak was discovered in the duration distribution, but disappeared when more data was accumulated. Balastegui et al. (2001) claimed the existence of a third class based on neural network classification. However, Hakkila et al. (2000, 2003) attributed the presence of this class to instrumental effects, and questioned its physical reality; this conclusion was also supported by Rajaniemi & Mähönen (2002), who employed an independent analysis method (self-organizing map, Kohonen 1982). The outputs of such unsupervised classifications are affected by several factors, e.g., the employed technique, specific samples and attributes used, among others (Hakkila et al. 2004), and by systematic biases (Roiger et al. 2000). Chattopadhyay et al. (2007) on the other hand used different clustering methods (K-means and Dirichlet process; the latter with an underlying assumption of a multinormal distribution), and again found statistical evidence for three GRB classes. Veres et al. (2010) claimed, based on the K-means method as well, to find evidence for the third class, too. The same approach turned out to be inconclusive for the *RHESSI* data (Řípa et al. 2012); on the other hand, multinormal fitting in the three-dimensional space of T_{90}, H and peak-count rates yielded three components.

Chattopadhyay & Maitra (2017) examined the complete BATSE data in a six-dimensional space of the same parameters as Mukherjee et al. (1998). By means of a multivariate Gaussian mixture model, they arrived at the conclusion that there are five clusters in this space. The same result was achieved by modeling with a multivariate Student-t distribution (Chattopadhyay & Maitra 2018, but see also Section 3.1 herein). Acuner & Ryde (2018) employed the Gaussian mixture model to analyze *Fermi* GRBs in a different space of the Band et al. (1993) spectral parameters (α, β, $E_{\rm peak}$), the duration T_{90} and the fluence, and also claimed evidence for five groups.

While not of direct importance herein, it is worth mentioning that the GRB family, besides short and long bursts, includes also ultra-long GRBs (Gendre et al. 2013; Levan et al. 2014; Zhang et al. 2014; Perna et al. 2018), low-luminosity GRBs (Bromberg et al. 2011), and short GRBs with extended emission (Norris & Bonnell 2006; Kaneko et al. 2015), i.e., having durations that would classify them as long GRBs, but without an associated supernova. They most likely originate from the merger of a white dwarf with an NS (King et al. 2007) or BH (Dong et al. 2018).

The aim of this work is to analyze the two most numerous GRB samples, the *CGRO*/BATSE and *Fermi*/GBM data sets, in the two-dimensional space of T_{90}–H, using mixtures of skewed distributions, in order to establish the number of GRB classes. This is the first attempt, except for that of Tarnopolski (2016b), to model GRB groups with skewed distributions,[1] and the first such approach in a bivariate scheme. In Section 2 the examined data sets and statistical methods together with the employed probability distributions are briefly described. Section 3 presents the results obtained for both GRB samples. Section 4 is devoted to discussion, and concluding remarks are gathered in Section 5. The `R` software[2] is utilized throughout; the fittings are performed with the package `mixsmsn`[3] (Prates et al. 2013).

[1] Skewed distributions have been, however, employed in other astrophysical applications, e.g., in modeling the mass distribution of neutron stars (Kiziltan et al. 2013).

[2] http://www.R-project.org/

[3] https://cran.r-project.org/web/packages/mixsmsn/index.html

2. Data Sets and Methods

2.1. Samples

The *Fermi* data set (Narayana Bhat et al. 2016) contains 1376 GRBs with measured both T_{90} and H_{32} (P. Veres 2018, private communication), where the hardness ratio $H_{32} = \frac{F_{50-300\,\mathrm{keV}}}{F_{10-50\,\mathrm{keV}}}$ is the ratio of fluences in the respective energy bands during the T_{90} interval. *CGRO*/BATSE[4] contains 1954 GRBs with T_{90} and H_{32}, where the hardness ratio is computed with slightly different energy bands: $H_{32} = \frac{F_{100-300\,\mathrm{keV}}}{F_{50-100\,\mathrm{keV}}}$.

2.2. Statistical Methods

2.2.1. Maximum Loglikelihood Fitting

Having a distribution[5] with a probability density function (PDF) given by $f = f(\boldsymbol{x};\,\theta)$ (possibly a mixture), where $\theta = \{\theta_i\}_{i=1}^{p}$ is a set of p parameters, the loglikelihood function is defined as

$$\mathcal{L}_p(\theta) = \sum_{i=1}^{N} \ln f(x_i;\,\theta), \tag{1}$$

where $\{\boldsymbol{x}_i\}_{i=1}^{N}$ are the data points from the sample to which a distribution is fitted. The fitting is performed by searching a set of parameters $\hat{\theta}$ for which the loglikelihood is maximized (Kendall & Stuart 1973). When nested models are considered, the maximal value of the loglikelihood function $\mathcal{L}_{p,\max} \equiv \mathcal{L}_p(\hat{\theta})$ increases when the number of parameters p increases.

2.2.2. Model Comparison—Information Criteria

For nested as well as non-nested models, the information criteria (IC): Akaike IC (AIC) and Bayesian IC (BIC) may be applied (Akaike 1974; Schwarz 1978; Burnham & Anderson 2004; Biesiada 2007; Liddle 2007; Tarnopolski 2016a, 2016b). They are defined as

$$\mathrm{AIC} = 2p - 2\mathcal{L}_{p,\max} \tag{2}$$

and

$$\mathrm{BIC} = p\ln N - 2\mathcal{L}_{p,\max}. \tag{3}$$

A preferred model is the one that minimizes AIC or BIC. The expressions for both IC consist of two competing terms: the first measuring the model complexity (number of free parameters) and the second measuring the goodness of fit (or more precisely, the lack thereof). The formulation of these IC penalizes the use of an excessive number of parameters. It prefers models with fewer parameters, as long as the others do not provide a substantially better fit. In the case of BIC, the penalization term is greater than the corresponding term from the AIC, $p\ln N > 2p$, for $N \geqslant 8$. Hence, the penalization in the case of the BIC is much more stringent, especially for large samples.

What is essential in assessing the goodness of fit in the AIC method is the difference, $\Delta_i = \mathrm{AIC}_i - \mathrm{AIC}_{\min}$. If $\Delta_i < 2$, then there is substantial support for the ith model (or the evidence against it is worth only a small mention), and the proposition that it is a proper description is highly probable. If $2 < \Delta_i < 4$, then there is strong support for the ith model. When $4 < \Delta_i < 7$, there is considerably less support, and models with $\Delta_i > 10$ have essentially no support (Burnham & Anderson 2004; Biesiada 2007). It is important to note that when two models with similar $\mathcal{L}_{\max}$ are considered, the Δ_i depends solely on the number of parameters due to the $2p$ term in Equation (2). Hence, when $\Delta_i/(2\Delta p) < 1$, the relative improvement is due to actual improvement of the fit, not to increasing the number of parameters only.

In the case of BIC, $\Delta_i = \mathrm{BIC}_i - \mathrm{BIC}_{\min}$, and the support for the ith model (or evidence against it) also depends on the differences: if $\Delta_i < 2$, then there is substantial support for the ith model. When $2 < \Delta_i < 6$, then there is positive evidence against the ith model. If $6 < \Delta_i < 10$, the evidence is strong, and models with $\Delta_i > 10$ yield very strong evidence against the ith model (essentially no support; Kass & Raftery 1995).

Despite apparent similarities between the AIC and BIC, it ought to be stressed that they answer different questions, as they are derived based on different assumptions. AIC tries to select a model that most adequately describes reality (in the form of the data under examination). This means that in fact the model being a real description of the data is never considered. On the contrary, BIC tries to find the true model among the set of candidates. Because BIC is more stringent, it has a tendency to underfit (resulting in an excessively simple model), while AIC, as a more liberal method, is inclined toward overfitting (accepting more parameters than needed). This may lead to pointing different models by the two criteria, which happens rarely, but is due to the fact that they try to satisfy different conditions.

2.3. Distributions

A mixture of n components, each having a PDF given by $f_i(\boldsymbol{x};\,\theta^{(i)})$, is defined as

$$f(\boldsymbol{x};\,\theta) = \sum_{i=1}^{n} A_i f_i(\boldsymbol{x};\,\theta^{(i)})$$

with the weights satisfying $\sum_{i=1}^{n} A_i = 1$, and $\theta = \bigcup_{i=1}^{n}\theta^{(i)}$. The following distributions are considered.

The multivariate, k-dimensional normal (Gaussian) distribution has a PDF:

$$\varphi_k(\boldsymbol{x};\,\boldsymbol{\mu},\,\boldsymbol{\Sigma}) = \frac{1}{\sqrt{(2\pi)^k|\boldsymbol{\Sigma}|}}\exp\left[-\frac{1}{2}(\boldsymbol{x}-\boldsymbol{\mu})^{\top}\boldsymbol{\Sigma}^{-1}(\boldsymbol{x}-\boldsymbol{\mu})\right], \tag{4}$$

where $\boldsymbol{\mu}$ is the location vector (which in this case is also the mean, because the distribution is not skewed), $\boldsymbol{\Sigma}$ is the covariance matrix, and $|\boldsymbol{\Sigma}| = \det\boldsymbol{\Sigma}$. In particular, for a bivariate case ($k = 2$),

$$\boldsymbol{\Sigma} = \begin{pmatrix} \sigma_x^2 & \rho\sigma_x\sigma_y \\ \rho\sigma_x\sigma_y & \sigma_y^2 \end{pmatrix}. \tag{5}$$

A mixture of n components is described by $p = 6n - 1$ free parameters.

The multivariate skew-normal ($\mathcal{SN}$) distribution (Azzalini & Capitanio 1999; Kollo et al. 2013; Prates et al. 2013) is given by

$$f_k^{(\mathcal{SN})}(\boldsymbol{x};\,\boldsymbol{\mu},\,\boldsymbol{\Sigma},\,\boldsymbol{\lambda}) = 2\varphi_k(\boldsymbol{x};\,\boldsymbol{\mu},\,\boldsymbol{\Sigma})\Phi(\boldsymbol{\lambda}^{\top}\boldsymbol{\Sigma}^{-1/2}(\boldsymbol{x}-\boldsymbol{\mu})), \tag{6}$$

[4] https://gammaray.nsstc.nasa.gov/batse/grb/catalog/current/

[5] Bivariate distributions are considered herein, but the methodology is applicable for any dimensionality of the data; see Tarnopolski (2016a, 2016b, 2016c) for a univariate analysis of T_{90}.

where $\Phi(.)$ denotes the CDF of a univariate standard normal distribution, and $\boldsymbol{\lambda}$ denotes the skewness parameter vector. If $\boldsymbol{\lambda} = 0$, then Equation (6) reduces to Equation (4). The mean of the $\mathcal{SN}$ distribution is $\boldsymbol{m} = \boldsymbol{\mu} + \sqrt{\frac{2}{\pi}}\frac{\boldsymbol{\Sigma\lambda}}{\sqrt{1+\boldsymbol{\lambda}^\top\boldsymbol{\Sigma\lambda}}}$, i.e., the location parameter $\boldsymbol{\mu}$ is not the mean itself, and the covariance is given by $\boldsymbol{\Sigma} - (\boldsymbol{m}-\boldsymbol{\mu})(\boldsymbol{m}-\boldsymbol{\mu})^\top$. The skewness[6] is nonzero unless $\boldsymbol{\lambda} = 0$. A mixture of n components is described by $p = 8n - 1$ free parameters.

The multivariate Student $t(\mathcal{T})$ distribution (Basso et al. 2010; Cabral et al. 2012; Prates et al. 2013) with ν degrees of freedom (dof) is defined to be

$$f_k^{(\mathcal{T})}(\boldsymbol{x};\,\boldsymbol{\mu},\,\boldsymbol{\Sigma},\,\nu) = \frac{1}{\sqrt{(\pi\nu)^k|\boldsymbol{\Sigma}|}}\frac{\Gamma\left(\frac{\nu+k}{2}\right)}{\Gamma\left(\frac{\nu}{2}\right)} \times\left(1+\frac{1}{\nu}(\boldsymbol{x}-\boldsymbol{\mu})^\top\boldsymbol{\Sigma}^{-1}(\boldsymbol{x}-\boldsymbol{\mu})\right)^{-\frac{\nu+k}{2}}, \tag{7}$$

where Γ is the gamma function. The mean (for $\nu > 1$) of the $\mathcal{T}$ distribution is $\boldsymbol{\mu}$, and the covariance matrix (for $\nu > 2$) is $\frac{\nu}{\nu-2}\boldsymbol{\Sigma}$. In the limit $\nu \to \infty$, the $\mathcal{T}$ distribution approaches the normal distribution from Equation (4). A mixture of n components is described by $p = 6n$ free parameters.

The multivariate skew-$\mathcal{T}$ ($\mathcal{ST}$) distribution (Cabral et al. 2012; Kollo et al. 2013; Prates et al. 2013) is defined as

$$f_k^{(\mathcal{ST})}(\boldsymbol{x};\,\boldsymbol{\mu},\,\boldsymbol{\Sigma},\,\nu,\,\boldsymbol{\lambda}) = 2f_k^{(\mathcal{T})}(\boldsymbol{x};\,\boldsymbol{\mu},\,\boldsymbol{\Sigma},\,\nu) \times T_{\nu+k}\left(\sqrt{\frac{\nu+k}{\nu+(\boldsymbol{x}-\boldsymbol{\mu})^\top\boldsymbol{\Sigma}^{-1}(\boldsymbol{x}-\boldsymbol{\mu})}}\,\boldsymbol{\lambda}^\top\boldsymbol{\Sigma}^{-1/2}(\boldsymbol{x}-\boldsymbol{\mu})\right), \tag{8}$$

where $T_{\nu+k}$ denotes the CDF of the standard univariate Student-t distribution with $(\nu + k)$ dof, and $\boldsymbol{\lambda}$ is the skewness parameter vector. Equation (8) reduces to Equation (7) for $\boldsymbol{\lambda} = 0$. In the limit $\nu \to \infty$, the $\mathcal{ST}$ distribution approaches the $\mathcal{SN}$ distribution from Equation (6). The mean (for $\nu > 1$) of the $\mathcal{ST}$ distribution is $\boldsymbol{m} = \boldsymbol{\mu} + \boldsymbol{\omega\xi}$, and its covariance (for $\nu > 2$) is $\frac{\nu}{\nu-2}\boldsymbol{\Sigma} - (\boldsymbol{m}-\boldsymbol{\mu})(\boldsymbol{m}-\boldsymbol{\mu})^\top$, where $\boldsymbol{\xi} = \sqrt{\frac{\nu}{\pi(1+\boldsymbol{\lambda}^\top\boldsymbol{\Sigma\lambda})}}\frac{\Gamma\left(\frac{\nu-1}{2}\right)}{\Gamma\left(\frac{\nu}{2}\right)}\boldsymbol{\Sigma\lambda}$ and $\boldsymbol{\omega} = \mathrm{diag}(\Sigma_{11},\ldots,\Sigma_{kk})^{1/2}$ (Azzalini & Capitanio 2003; Kollo et al. 2013). The skewness (for $\nu > 3$) is nonzero unless $\boldsymbol{\lambda} = 0$. A mixture of n components is described by $p = 8n$ free parameters.

The distributions are referred to as 2G and 3G for the mixture of two and three Gaussian components, respectively; $2\mathcal{SN}$ and $3\mathcal{SN}$ for the respective mixtures of $\mathcal{SN}$ distributions; $2\mathcal{T}$ and $3\mathcal{T}$ in case of the $\mathcal{T}$ distribution; and $2\mathcal{ST}$ and $3\mathcal{ST}$ for the $\mathcal{ST}$ distribution.

3. Results

3.1. BATSE

Results of the fittings performed with the set of 1954 BATSE GRBs are displayed in graphical form in Figure 1, whereas the obtained parameters are gathered in Table 1, which also contains the values of $\mathcal{L}_{\max}$, ΔAIC, and ΔBIC. The BATSE data set consists of $\sim$25% of short GRBs, forming a cloud distinct from the long GRBs in the T_{90}–H_{32} plane, making the two-component fits consistent with each other qualitatively, as follows from the left column of Figure 1. Likewise, for all statistical models considered, the introduction of a third component placed it roughly between the two major classes, without significantly affecting them. The ΔAIC and ΔBIC values, sorted in increasing order, are additionally gathered in Table 2 for clarity, with a graphical representation in Figure 2. It follows that the AIC points at the $3\mathcal{T}$ model as the one that best describes the data, with the $2\mathcal{ST}$ in the second position. Due to the $\Delta\mathrm{AIC} = 3.6$, the support for the latter is strong. On the other hand, the BIC points at $2\mathcal{ST}$ as the best model, with the $3\mathcal{T}$ with weak support ($\Delta\mathrm{BIC} = 7.56$). Given that the AIC (BIC) has a tendency toward overfitting (underfitting), and that the goal herein is to obtain the simplest model possible that adequately describes the data, overall the $2\mathcal{ST}$ model is more likely to underly the observations.

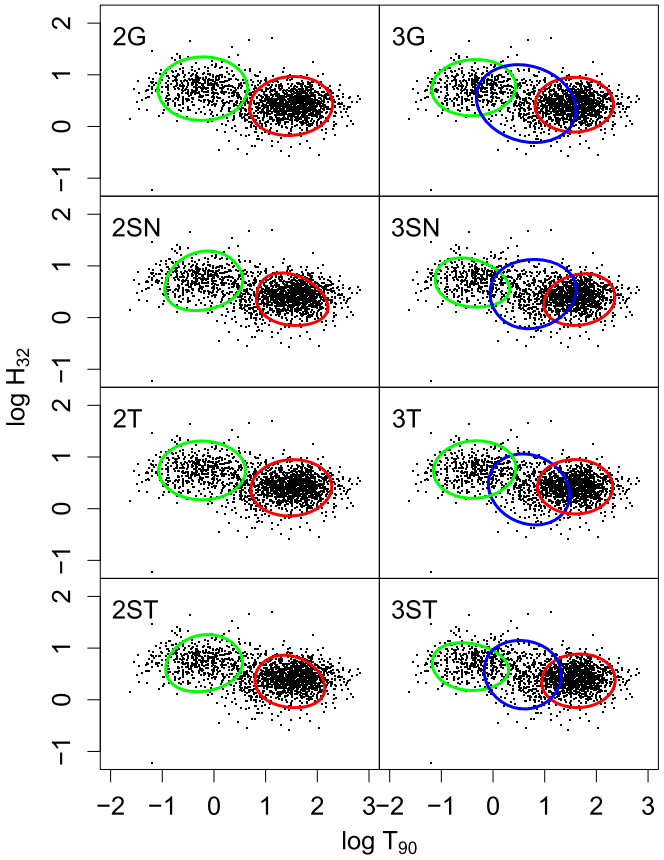

Figure 1. Fits to the BATSE data. The contours depict the FWHM of each component, and T_{90} is measured in seconds.

Within the AIC framework, the $3\mathcal{ST}$ model (the most complex among those examined, with $p = 24$ free parameters) is barely worth mentioning ($\Delta\mathrm{AIC} = 9.8$), with the remaining models—in the BIC framework as well—confidently rejected. In particular, the 2G is the worst model in both schemes, and the celebrated 3G is characterized with both ΔAIC and ΔBIC well above the value of 10. It is curious that the mixtures of the simplest skewed model—the $\mathcal{SN}$—perform rather poorly (compare to Tarnopolski 2016b).

[6] Multivariate measures of skewness are not as unambiguous as in the univariate case (Balakrishnan & Scarpa 2012), hence no explicit formulae are given herein.

Table 1
Parameters of the Fits to the BATSE Data

Model	A	$\boldsymbol{\mu}$	$\boldsymbol{\Sigma}$	$\boldsymbol{\lambda}$	ν	$\mathcal{L}_{\max}$	ΔAIC	ΔBIC	p
2G	0.283	(−0.220, 0.732)	$\begin{pmatrix}0.543 & 0.005\\0.005 & 0.274\end{pmatrix}$	⋯	⋯	−2415.561	115.918	90.011	11
	0.717	(1.494, 0.397)	$\begin{pmatrix}0.466 & 0.019\\0.019 & 0.236\end{pmatrix}$	⋯					
	0.198	(−0.374, 0.752)	$\begin{pmatrix}0.476 & 0.017\\0.017 & 0.214\end{pmatrix}$	⋯					
3G	0.189	(0.643, 0.442)	$\begin{pmatrix}0.671 & -0.087\\-0.087 & 0.409\end{pmatrix}$	⋯	⋯	−2359.336	15.469	23.028	17
	0.613	(1.570, 0.423)	$\begin{pmatrix}0.416 & 0.004\\0.004 & 0.203\end{pmatrix}$	⋯					
2SN	0.301	(−0.734, 0.836)	$\begin{pmatrix}0.857 & -0.069\\-0.069 & 0.272\end{pmatrix}$	(1.923, −0.651)	⋯	−2377.601	47.998	44.402	15
	0.699	(1.866, 0.584)	$\begin{pmatrix}0.585 & 0.104\\0.104 & 0.291\end{pmatrix}$	(−1.615, −1.425)					
	0.196	(−0.091, 0.912)	$\begin{pmatrix}0.548 & 0.074\\0.074 & 0.259\end{pmatrix}$	(−1.244, −1.396)					
3SN	0.228	(1.218, 0.158)	$\begin{pmatrix}0.807 & -0.181\\-0.181 & 0.467\end{pmatrix}$	(−1.203, 0.985)	⋯	−2354.469	17.733	58.758	23
	0.576	(1.378, 0.516)	$\begin{pmatrix}0.455 & -0.028\\-0.028 & 0.218\end{pmatrix}$	(0.852, −0.683)					
2T	0.277	(−0.231, 0.740)	$\begin{pmatrix}0.508 & -0.001\\-0.001 & 0.233\end{pmatrix}$	⋯	11.195	−2382.350	49.497	23.59	12
	0.723	(1.496, 0.404)	$\begin{pmatrix}0.441 & 0.016\\0.016 & 0.214\end{pmatrix}$	⋯					
	0.226	(−0.355, 0.758)	$\begin{pmatrix}0.458 & 0.016\\0.016 & 0.223\end{pmatrix}$	⋯					
3T	0.156	(0.697, 0.372)	$\begin{pmatrix}0.446 & -0.061\\-0.061 & 0.340\end{pmatrix}$	⋯	16.391	−2351.602	0.	7.558	18
	0.618	(1.588, 0.425)	$\begin{pmatrix}0.383 & -0.002\\-0.002 & 0.200\end{pmatrix}$	⋯					
2ST	0.291	(−0.686, 0.830)	$\begin{pmatrix}0.752 & -0.056\\-0.056 & 0.247\end{pmatrix}$	(1.591, −0.569)	12.089	−2355.400	3.596	0.	16
	0.709	(1.850, 0.531)	$\begin{pmatrix}0.552 & 0.069\\0.069 & 0.240\end{pmatrix}$	(−1.361, −0.877)					
	0.194	(−0.230, 0.924)	$\begin{pmatrix}0.471 & 0.056\\0.056 & 0.271\end{pmatrix}$	(−0.715, −1.462)					
3ST	0.196	(0.985, 0.231)	$\begin{pmatrix}0.628 & -0.167\\-0.167 & 0.411\end{pmatrix}$	(−1.025, 0.641)	21.494	−2350.503	9.802	50.827	24
	0.610	(1.484, 0.479)	$\begin{pmatrix}0.397 & -0.010\\-0.010 & 0.208\end{pmatrix}$	(0.370, −0.335)					

Table 2
The Δ_i's (AIC and BIC), in Increasing Order, of the Examined Models for the BATSE Data Set

Model	ΔAIC	Model	ΔBIC
3T	0.	2ST	0.
2ST	3.596	3T	7.558
3ST	9.802	3G	23.028
3G	15.469	2T	23.590
3SN	17.733	2SN	44.402
2SN	47.998	3ST	50.827
2T	49.497	3SN	58.758
2G	115.918	2G	90.011

3.2. Fermi

In the same manner the 1376 *Fermi* GRBs were analyzed. The resulting parameters are gathered in Table 3 and the fits are displayed in Figure 3. The two-component models are

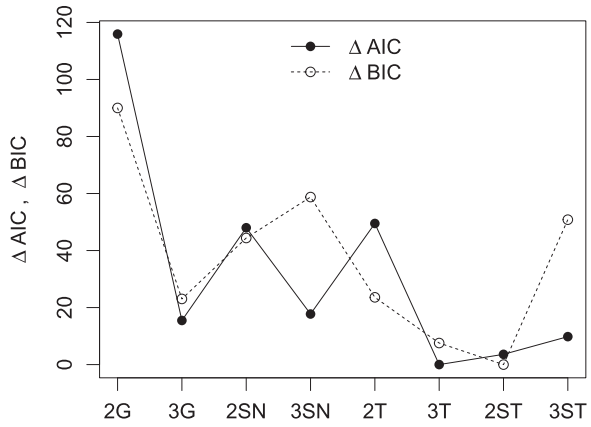

Figure 2. Information criteria scores for the BATSE data.

Table 3
Parameters of the Fits to the *Fermi* Data

Model	A	$\boldsymbol{\mu}$	$\boldsymbol{\Sigma}$	$\boldsymbol{\lambda}$	ν	$\mathcal{L}_{\max}$	ΔAIC	ΔBIC	p
2G	0.221	(0.025, 0.213)	$\begin{pmatrix} 0.558 & -0.107 \\ -0.107 & 0.446 \end{pmatrix}$	⋯	⋯	−1525.740	106.571	85.663	11
	0.779	(1.466, −0.196)	$\begin{pmatrix} 0.455 & -0.019 \\ -0.019 & 0.217 \end{pmatrix}$	⋯					
	0.009	(−0.248, 1.137)	$\begin{pmatrix} 0.383 & 0.208 \\ 0.208 & 0.903 \end{pmatrix}$	⋯					
3G	0.227	(0.078, 0.134)	$\begin{pmatrix} 0.556 & -0.151 \\ -0.151 & 0.356 \end{pmatrix}$	⋯	⋯	−1478.543	24.177	34.631	17
	0.764	(1.483, −0.191)	$\begin{pmatrix} 0.443 & -0.020 \\ -0.020 & 0.222 \end{pmatrix}$	⋯					
2SN	0.234	(−0.124, −0.162)	$\begin{pmatrix} 0.614 & -0.049 \\ -0.049 & 0.579 \end{pmatrix}$	(1.367, 2.359)	⋯	−1499.467	62.024	60.956	15
	0.766	(1.295, −0.211)	$\begin{pmatrix} 0.483 & -0.016 \\ -0.016 & 0.215 \end{pmatrix}$	(0.553, 0.161)					
	0.094	(−0.489, 0.038)	$\begin{pmatrix} 0.367 & 0.070 \\ 0.070 & 0.615 \end{pmatrix}$	(617.885, 1782.993)					
3SN	0.581	(1.378, −0.251)	$\begin{pmatrix} 0.461 & -0.000 \\ -0.000 & 0.208 \end{pmatrix}$	(0.812, 0.434)	⋯	−1470.025	19.141	60.956	23
	0.325	(1.457, −0.318)	$\begin{pmatrix} 0.875 & -0.177 \\ -0.177 & 0.345 \end{pmatrix}$	(−3.203, 1.058)					
2T	0.187	(−0.114, 0.260)	$\begin{pmatrix} 0.452 & -0.088 \\ -0.088 & 0.327 \end{pmatrix}$	⋯	12.118	−1497.100	49.29	28.383	12
	0.813	(1.445, -0.195)	$\begin{pmatrix} 0.445 - 0.018 \\ -0.018 \quad 0.212 \end{pmatrix}$	⋯					
	0.170	(−0.183, 0.290)	$\begin{pmatrix} 0.408 & -0.071 \\ -0.071 & 0.304 \end{pmatrix}$	⋯					
3T	0.494	(1.195, −0.151)	$\begin{pmatrix} 0.392 & -0.012 \\ -0.012 & 0.225 \end{pmatrix}$	⋯	9.318	−1483.156	33.403	43.857	18
	0.336	(1.754, −0.247)	$\begin{pmatrix} 0.320 & 0.012 \\ 0.012 & 0.177 \end{pmatrix}$	⋯					
2ST	0.121	(−0.423, 0.059)	$\begin{pmatrix} 0.365 & 0.022 \\ 0.022 & 0.449 \end{pmatrix}$	(2.552, 7.09)	11.746	−1468.454	0.	0.	16
	0.879	(1.869, −0.312)	$\begin{pmatrix} 0.699 & -0.090 \\ -0.090 & 0.239 \end{pmatrix}$	(−1.854, 0.797)					
	0.124	(−0.414, 0.060)	$\begin{pmatrix} 0.368 & 0.019 \\ 0.019 & 0.447 \end{pmatrix}$	(2.355, 6.746)					
3ST	0.390	(1.502, −0.239)	$\begin{pmatrix} 0.671 & -0.074 \\ -0.074 & 0.247 \end{pmatrix}$	(−7.253, 0.421)	11.803	−1463.872	6.836	48.651	24
	0.486	(1.888, −0.298)	$\begin{pmatrix} 0.390 & -0.047 \\ -0.047 & 0.216 \end{pmatrix}$	(−0.765, 0.648)					

consistent with each other, just like most of the three-component models. A clear exception is the 3G fit, where the third component is not placed between the short and long GRBs, but drifts toward the harder part of the short GRBs' cluster. Setting different starting values for the fitting procedure or restricting the available range of parameters to force an outcome similar to the one obtained in the case of BATSE data did not result in a quality fit—the AIC and BIC values were at best by a few hundreds greater than for the other models. The *Fermi* data set contains ∼15% of short GRBs—this results in about half as many short GRBs as in the BATSE sample, which are also more sparse and spread out on the T_{90}–H_{32} plane. Hence the weight of these points is high enough for the maximum loglikelihood procedure to take them into account when fitting.

Nonetheless, as follows from the Δ_i values from Figure 4 and Table 4, the 2G model is again the worst among those examined, and the 3G is off the rate with Δ_i much higher than 10. Both AIC and BIC unanimously point at the $2\mathcal{ST}$ as the best description of the data. In terms of BIC no other model is even competitive, while there is moderate support for the $3\mathcal{ST}$ in terms of AIC ($\Delta_i = 6.84$). Overall, the $2\mathcal{ST}$ is again the best description of the observed (T_{90}, H_{32}) data points in the logarithmic plane. Note also that it has a comparable number of free components (16 versus 17) to the previously broadly employed 3G, but does not invoke a new class of GRBs.

4. Discussion

To date, all parametric analyses of the GRB population in the T_{90}–H_{32} plane were conducted by means of the Gaussian mixture model. On this basis, the existence of a third class of GRBs, intermediate in durations and with soft spectra, has been claimed several times (see Section 1). However, a similar claim based on the log T_{90} distribution alone was refuted by showing that the observed durations are better fitted by only two skewed components rather than three Gaussian ones (Tarnopolski 2015c, 2016b, 2016c). The first to notice that the employment

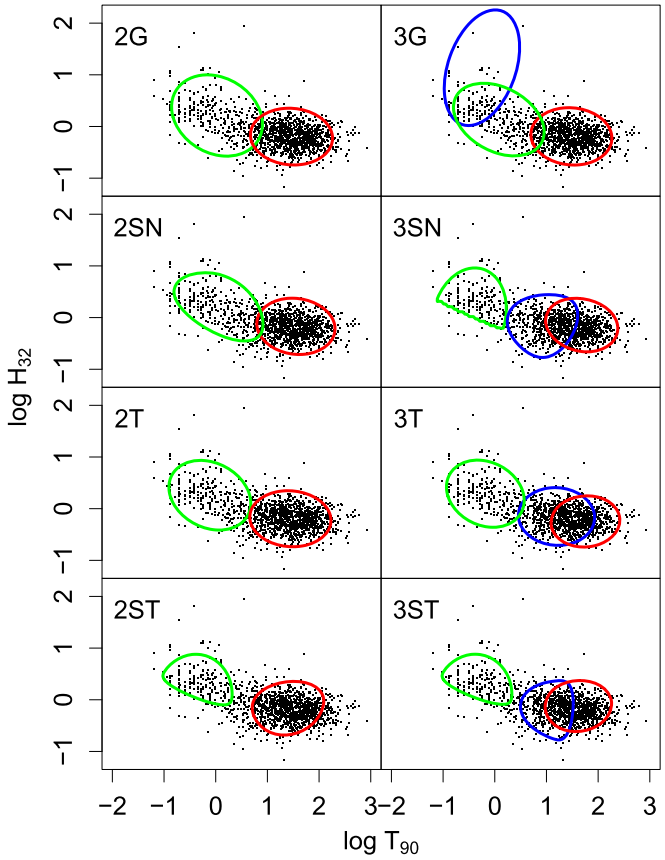

Figure 3. Fits to the *Fermi* data. The contours depict the FWHM of each component, and T_{90} is measured in seconds.

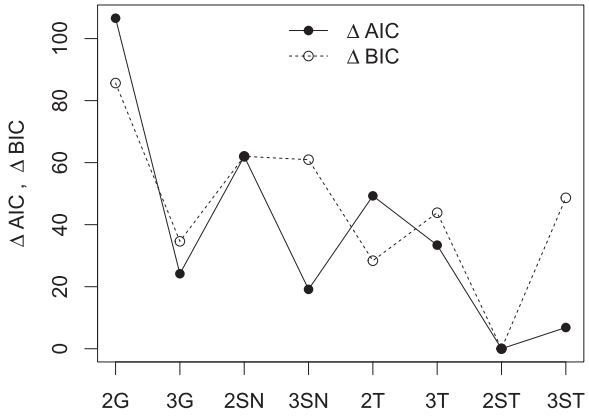

Figure 4. Information criteria scores for the *Fermi* data.

Table 4
The Δ_i's (AIC and BIC), in Increasing Order, of the Examined Models for the *Fermi* Data Set

Model	ΔAIC	Model	ΔBIC
2ST	0.	2ST	0.
3ST	6.836	2T	28.383
3SN	19.141	3G	34.631
3G	24.177	3T	43.857
3T	33.403	3ST	48.651
2T	49.290	3SN	60.956
2SN	62.024	2SN	62.024
2G	106.571	2G	85.663

of Gaussian distributions is not fully justified were Koen & Bere (2012), who wrote:[7] "There is no guarantee that the components of a mixture correspond to physically distinct classes of objects. It is entirely possible that the distributions of class properties, such as log T_{90}, are non-normal: in such a case, spurious classes would be identified due to the modeling of a non-normal distribution by normal components." Additionally, they showed in their Figure 14 two fits to *Swift* duration data that are very similar to each other, yet composed of entirely different components. Hence the association of a component of a statistical mixture to a physical class of objects and the inference of their properties is a dubious approach. Zitouni et al. (2015) later suggested that the asymmetry in the duration distribution might come from a possible asymmetric distribution of the progenitor envelope mass. In this spirit, four bivariate statistical models (Section 2.3) were tested herein: the Gaussian one, its skewed version (the $\mathcal{SN}$ distribution), the Student distribution, $\mathcal{T}$ (which, while being symmetric like the normal distribution, has a wider spread and a more slender shape), and its skewed version (the $\mathcal{ST}$ distribution). It was found (Section 3) that despite, rather surprisingly, the mixture of $\mathcal{SN}$ distributions not being competitive with the Gaussian model (contrary to the univariate case; Tarnopolski 2016b), the $2\mathcal{ST}$ is the best description of the data among the examined possibilities. Particularly, it is a significant improvement of the fit compared to the 3G. The IC also indicate that the $3\mathcal{ST}$ model is excessive. It should be emphasized that if the empirical distributions were not inherently skewed, this would be reflected in the fitting by obtaining $\boldsymbol{\lambda} \approx 0$ at least for some components of the mixtures, but this is not the case for either the $\mathcal{SN}$, or the $\mathcal{ST}$ models, regardless of the number of components employed (i.e., two or three). Therefore, the results imply that the existence of the presumed third GRB class, as a fundamentally distinct one from the short and long ones, is unlikely. On one hand, it concords with the possibility that this class may be in fact attributed, at least partially, to X-ray flashes (XRFs, Heise et al. 2001; Heise 2003; Kippen et al. 2003; Sakamoto et al. 2005) related to long GRBs (Sakamoto et al. 2008), and hence constitute the tail of the long GRBs group (Řípa & Mészáros 2014, 2016), especially in the case of *Swift* GRBs (Veres et al. 2010; but see also the discussion in Řípa & Mészáros 2016). On the other hand, the presumed third class of GRBs, as observed by *RHESSI*, is not located at the soft tail of long GRBs, but between the short and long ones, hence it is on average harder than XRFs (Řípa et al. 2012). In fact, their hardness ratios are comparable to those of short GRBs (Řípa & Mészáros 2016). The smallest fraction of GRBs consistent with the definition of XRFs is in the BATSE catalog (Řípa & Mészáros 2016). This shows that the intermediate class is indeed elusive, and its characteristics—in particular the location in the T_{90}–H plane—are strongly detector-dependent, so any claims about its physical properties should be taken with caution.

The instrumental effects cannot be neglected in discussing the properties of GRB classes (Tarnopolski 2015c; Řípa & Mészáros 2016). *Swift* is more sensitive in soft bands compared

[7] However, Mukherjee et al. (1998) noted that "the distributions often seem bimodal with asymmetrical non-Gaussian shapes," but failed to employ skewed distributions in modeling and proceeded considering "the hypothesis that the sample consists of two or more distinct classes" by assuming multinormal distributions.

to BATSE, hence it is more inclined toward detecting long GRBs and its low-luminosity tail—the putative intermediate class—than short ones. *BeppoSAX* is also more sensitive to long GRBs (Horváth 2009), hence the lack of a distinct short GRB peak in the duration distribution. On the other hand, *Fermi* is more sensitive at very soft and very hard GRBs, yet a soft-intermediate tail of long GRBs is not visible in Figure 3—but the third component in the 3G model stretches from the short GRBs toward even higher hardness ratios. Except for this, in both BATSE and *Fermi* the third component is being located between the short and long groups, with typical hardness similar to long GRBs', especially in the case of *Fermi* (Figures 1 and 3). Different energy-detection intervals (e.g., 15–150 keV for *Swift*, and 8–1000 keV for *Fermi*) lead to contrasting group characteristics. *Suzaku*'s energy range (50–5000 keV) makes the resulting T_{90} distribution similar to those of BATSE and *Fermi* rather than *Swift* (Ohmori et al. 2016). Also, different energy sensitivities of the detectors give different estimates of T_{90}, and the flux limit for detection introduces a selection bias. Likewise, there are known observational and instrumental selection effects (Coward et al. 2013) related with the redshift distribution (Mészáros et al. 2006) that affect the observed GRB samples. Finally, the spectrum of a GRB depends on the detector (Sakamoto et al. 2011), which in turn affects the calculated hardness ratio. Overall, the distinction between short and long GRBs—on observational, statistical, and astrophysical grounds—is firm. The presumed third—intermediate in duration—class is putative, and there is no need to invoke it to describe the observed distributions of GRB properties. Lastly, a more flexible model, given by a mixture of copulas (Koen & Bere 2017), would allow us to separately model the marginals of a multivariate distribution, taking account of physical constraints on each variable independently.

Ideally, it is desirable to have the exact shape of the observed distributions derived from a physical theory, which has not been convincingly realized. However, as the 2G is better than 3G in the rest frame (Huja et al. 2009; Tarnopolski 2016a; Zhang et al. 2016; Kulkarni & Desai 2017), and competitive with skewed models (Tarnopolski 2016c) in the univariate case of $\log T_{90}$, it is hereby suggested that the redshift distribution of GRBs (Natarajan et al. 2005; Mészáros et al. 2006, 2011; Li 2008; Le & Mehta 2017) is crucial in explaining the skewness of the observed quantities (M. Tarnopolski 2018, in preparation). Some works (Mukherjee et al. 1998; Roiger et al. 2000; Balastegui et al. 2001; Chattopadhyay et al. 2007; Řípa et al. 2012; Chattopadhyay & Maitra 2017, 2018; Acuner & Ryde 2018) have claimed to find three and more GRB groups in high dimensional parameter spaces. Such an approach must be undertaken with care, as (i) principal component analyses usually pointed at three variables (Bagoly et al. 1998; Borgonovo & Björnsson 2006; Bagoly et al. 2009; Horvath et al. 2012; Chattopadhyay & Maitra 2017; Acuner & Ryde 2018), and (ii) higher dimensional spaces become more and more capacious, hence the identification of, e.g., five clusters might be spurious.

5. Summary

1. Mixtures of two and three components of bivariate distributions: Gaussian, skew-normal ($\mathcal{SN}$), Student t ($\mathcal{T}$), and skew-t ($\mathcal{ST}$), were fitted to the $\log T_{90}-\log H_{32}$ data of *CGRO*/BATSE and *Fermi*/GBM.
2. Information criteria (AIC and BIC) were used to establish that the $2\mathcal{ST}$ model is significantly better at describing the data than any other among the considered ones.
3. This is evidence for the nonexistence of the elusive third, intermediate in durations and with soft spectra, class of GRBs.
4. The distributions of the GRBs' observed parameters are likely to be intrinsically skewed, possibly by the intrinsic skewness of the parameters governing the physical mechanism of a GRB.
5. It is suggested that the redshift distribution plays a crucial role in explaining the skewness of the parameters in the observer frame.

The author is grateful to Peter Veres for providing the hardness ratios of *Fermi*/GBM GRBs, and wishes to thank Jakub Řípa for comments on the manuscript. The final version of this manuscript was concluded during a visit at the Astronomical Institute of Charles University, Prague, Czech Republic. Support by the Polish National Science Center through an OPUS grant No. 2017/25/B/ST9/01208 is acknowledged.

Software: `R` (http://www.R-project.org/), `mixsmsn` (Prates et al. 2013, https://cran.r-project.org/web/packages/mixsmsn/index.html).

ORCID iDs

Mariusz Tarnopolski https://orcid.org/0000-0003-4666-0154

References

Abbott, B. P., Abbott, R., Abbott, T. D., et al. 2017a, ApJL, 848, L12
Abbott, B. P., Abbott, R., Abbott, T. D., et al. 2017b, ApJL, 848, L13
Acuner, Z., & Ryde, F. 2018, MNRAS, 475, 1708
Akaike, H. 1974, ITAC, 19, 716
Azzalini, A., & Capitanio, A. 1999, J.R. Statist. Soc. B, 61, 579
Azzalini, A., & Capitanio, A. 2003, J.R. Statist. Soc. B, 65, 367
Bagoly, Z., Borgonovo, L., Mészáros, A., Balázs, L. G., & Horváth, I. 2009, A&A, 493, 51
Bagoly, Z., Mészáros, A., Horváth, I., Balázs, L. G., & Mészáros, P. 1998, ApJ, 498, 342
Balakrishnan, N., & Scarpa, B. 2012, Journal of Multivariate Analysis, 104, 73
Balastegui, A., Ruiz-Lapuente, P., & Canal, R. 2001, MNRAS, 328, 283
Band, D., Matteson, J., Ford, L., et al. 1993, ApJ, 413, 281
Basso, R. M., Lachos, V. H., Cabral, C. R. B., & Ghosh, P. 2010, Comput. Stat. Data Anal., 54, 2926
Biesiada, M. 2007, JCAP, 2, 003
Borgonovo, L., & Björnsson, C.-I. 2006, ApJ, 652, 1423
Bromberg, O., Nakar, E., & Piran, T. 2011, ApJL, 739, L55
Bromberg, O., Nakar, E., Piran, T., & Sari, R. 2013, ApJ, 764, 179
Burnham, K. P., & Anderson, D. R. 2004, Sociological Methods Research, 33, 261
Bystricky, P., Meszaros, A., & Ripa, J. 2012, in Proc. 21st Annual Conf. of Doctoral Students—WDS 2012, ed. J. Safrankova & J. Pavlu (Prague: MATFYZPRESS), 129
Cabral, C. R. B., Lachos, V. H., & Prates, M. O. 2012, Computational Statistics Data Analysis, 56, 126
Cano, Z., Wang, S.-W., Dai, Z.-G., & Wu, X.-F. 2017, AdAst, 2017, 8929054
Chattopadhyay, S., & Maitra, R. 2017, MNRAS, 469, 3374
Chattopadhyay, S., & Maitra, R. 2018, MNRAS, 481, 3196
Chattopadhyay, T., Misra, R., Chattopadhyay, A. K., & Naskar, M. 2007, ApJ, 667, 1017
Coward, D. M., Howell, E. J., Branchesi, M., et al. 2013, MNRAS, 432, 2141
de Ugarte Postigo, A., Horváth, I., Veres, P., et al. 2011, A&A, 525, A109
Dong, Y.-Z., Gu, W.-M., Liu, T., & Wang, J. 2018, MNRAS, 475, L101
Kass, R. E., & Raftery, A. E. 1995, J. Am. Stat. Assoc., 90, 773
Eichler, D., Livio, M., Piran, T., & Schramm, D. N. 1989, Natur, 340, 126
Filippenko, A. V. 1997, ARA&A, 35, 309
Frontera, F., Guidorzi, C., Montanari, E., et al. 2009, ApJS, 180, 192

Fynbo, J. P. U., Watson, D., Thöne, C. C., et al. 2006, Natur, 444, 1047
Galama, T. J., Vreeswijk, P. M., van Paradijs, J., et al. 1998, Natur, 395, 670
Gendre, B., Stratta, G., Atteia, J. L., et al. 2013, ApJ, 766, 30
Goldstein, A., Veres, P., Burns, E., et al. 2017, ApJL, 848, L14
Gruber, D., Goldstein, A., Weller von Ahlefeld, V., et al. 2014, ApJS, 211, 12
Hakkila, J., Giblin, T. W., Roiger, R. J., et al. 2003, ApJ, 582, 320
Hakkila, J., Giblin, T. W., Roiger, R. J., et al. 2004, BaltA, 13, 211
Hakkila, J., Haglin, D. J., Pendleton, G. N., et al. 2000, ApJ, 538, 165
Heise, J. 2003, in AIP Conf. Ser. 662, Gamma-Ray Burst and Afterglow Astronomy 2001: A Workshop Celebrating the First Year of the HETE Mission, ed. G. R. Ricker & R. K. Vanderspek (New York: AIP Publishing), 229
Heise, J., Zand, J. I., Kippen, R. M., & Woods, P. M. 2001, in Gamma-ray Bursts in the Afterglow Era, ed. E. Era, F. Costa, & J. Frontera (Berlin: Springer), 16
Hjorth, J., Sollerman, J., Møller, P., et al. 2003, Natur, 423, 847
Horváth, I. 1998, ApJ, 508, 757
Horváth, I. 2002, A&A, 392, 791
Horváth, I. 2009, Ap&SS, 323, 83
Horváth, I., Bagoly, Z., Balázs, L. G., et al. 2010, ApJ, 713, 552
Horváth, I., Balázs, L. G., Bagoly, Z., Ryde, F., & Mészáros, A. 2006, A&A, 447, 23
Horváth, I., Balázs, L. G., Bagoly, Z., & Veres, P. 2008, A&A, 489, L1
Horvath, I., Balázs, L. G., Hakkila, J., Bagoly, Z., & Preece, R. D. 2012, in Gamma-Ray Bursts 2012 Conf. (GRB 2012), 46
Horváth, I., Tóth, B. G., Hakkila, J., et al. 2018, Ap&SS, 363, 53
Huja, D., Mészáros, A., & Řípa, J. 2009, A&A, 504, 67
Kaneko, Y., Bostancı, Z. F., Göğüş, E., & Lin, L. 2015, MNRAS, 452, 824
Kann, D. A., Klose, S., Zhang, B., et al. 2011, ApJ, 734, 96
Kendall, M., & Stuart, A. 1973, The Advanced Theory of Statistics (3rd ed.; London: Griffin)
King, A., Olsson, E., & Davies, M. B. 2007, MNRAS, 374, L34
Kippen, R. M., Woods, P. M., Heise, J., et al. 2003, in AIP Conf. Ser. 662, Gamma-Ray Burst and Afterglow Astronomy 2001: A Workshop Celebrating the First Year of the HETE Mission, ed. G. R. Ricker & R. K. Vanderspek, 244
Kiziltan, B., Kottas, A., De Yoreo, M., & Thorsett, S. E. 2013, ApJ, 778, 66
Klebesadel, R. W., Strong, I. B., & Olson, R. A. 1973, ApJL, 182, L85
Koen, C., & Bere, A. 2012, MNRAS, 420, 405
Koen, C., & Bere, A. 2017, MNRAS, 471, 2771
Kohonen, T. 1982, Biological Cybernetics, 43, 59
Kollo, T., Selart, A., & Visk, H. 2013, in From Multivariate Skewed Distributions to Copulas, ed. R. B. Bapat et al. (India: Springer India), 63
Koshut, T. M., Paciesas, W. S., Kouveliotou, C., et al. 1996, ApJ, 463, 570
Kouveliotou, C., Koshut, T., Briggs, M. S., et al. 1996, in AIP Conf. Ser. 384, Gamma-ray bursts: 3rd Huntsville symposium, ed. C. Kouveliotou, M. F. Briggs, & G. J. Fishman (New York: AIP), 42
Kouveliotou, C., Meegan, C. A., Fishman, G. J., et al. 1993, ApJL, 413, L101
Kulkarni, S., & Desai, S. 2017, Ap&SS, 362, 70
Kwong, H. S., & Nadarajah, S. 2018, MNRAS, 473, 625
Le, T., & Mehta, V. 2017, ApJ, 837, 17
Levan, A. J., Tanvir, N. R., Starling, R. L. C., et al. 2014, ApJ, 781, 13
Li, L.-X. 2008, MNRAS, 388, 1487
Li, Y., Zhang, B., & Lü, H.-J. 2016, ApJS, 227, 7
Liddle, A. R. 2007, MNRAS, 377, L74
MacFadyen, A. I., & Woosley, S. E. 1999, ApJ, 524, 262
Mazets, E. P., Golenetskii, S. V., Ilinskii, V. N., et al. 1981, Ap&SS, 80, 3
McBreen, B., Hurley, K. J., Long, R., & Metcalfe, L. 1994, MNRAS, 271, 662
Meegan, C. A., Fishman, G. J., Wilson, R. B., et al. 1992, Natur, 355, 143
Mészáros, A., Bagoly, Z., Balázs, L. G., & Horváth, I. 2006, A&A, 455, 785
Mészáros, A., Řípa, J., & Ryde, F. 2011, A&A, 529, A55
Mukherjee, S., Feigelson, E. D., Jogesh Babu, G., et al. 1998, ApJ, 508, 314
Nakar, E. 2007, PhR, 442, 166
Narayan, R., Paczynski, B., & Piran, T. 1992, ApJL, 395, L83
Narayana Bhat, P., Meegan, C. A., von Kienlin, A., et al. 2016, ApJS, 223, 28
Natarajan, P., Albanna, B., Hjorth, J., et al. 2005, MNRAS, 364, L8
Norris, J. P., & Bonnell, J. T. 2006, ApJ, 643, 266
Ohmori, N., Yamaoka, K., Ohno, M., et al. 2016, PASJ, 68, S30
Paciesas, W. S., Meegan, C. A., Pendleton, G. N., et al. 1999, ApJS, 122, 465
Paczynski, B. 1991, AcA, 41, 257
Paczyński, B. 1998, ApJL, 494, L45
Perna, R., Lazzati, D., & Cantiello, M. 2018, ApJ, 859, 48
Prates, M., Lachos, V., & Cabral, C. B. 2013, Journal of Statistical Software, 54, 1
Rajaniemi, H. J., & Mähönen, P. 2002, ApJ, 566, 202
Řípa, J., & Mészáros, A. 2014, in Proc. of Swift: 10 Years of Discovery (SWIFT 10), ed. P. Caraveo et al. (Rome, Italy), 103
Řípa, J., & Mészáros, A. 2016, Ap&SS, 361, 370
Řípa, J., Mészáros, A., Veres, P., & Park, I. H. 2012, ApJ, 756, 44
Řípa, J., Mészáros, A., Wigger, C., et al. 2009, A&A, 498, 399
Roiger, R. J., Hakkila, J., Haglin, D. J., Pendleton, G. N., & Mallozzi, R. S. 2000, in AIP Conf. Ser. 526, Gamma-ray Bursts, 5th Huntsville Symp., ed. R. M. Kippen, R. S. Mallozzi, & G. J. Fishman, 38
Ruffini, R., Rueda, J. A., Muccino, M., et al. 2016, ApJ, 832, 136
Sakamoto, T., Hullinger, D., Sato, G., et al. 2008, ApJ, 679, 570
Sakamoto, T., Lamb, D. Q., Kawai, N., et al. 2005, ApJ, 629, 311
Sakamoto, T., Pal'Shin, V., Yamaoka, K., et al. 2011, PASJ, 63, 215
Savchenko, V., Ferrigno, C., Kuulkers, E., et al. 2017, ApJL, 848, L15
Schwarz, G. 1978, Ann. Statist., 6, 461
Stanek, K. Z., Matheson, T., Garnavich, P. M., et al. 2003, ApJL, 591, L17
Tanvir, N. R., Levan, A. J., Fruchter, A. S., et al. 2013, Natur, 500, 547
Tarnopolski, M. 2015a, Ap&SS, 359, 20
Tarnopolski, M. 2015b, MNRAS, 454, 1132
Tarnopolski, M. 2015c, A&A, 581, A29
Tarnopolski, M. 2016a, NewA, 46, 54
Tarnopolski, M. 2016b, MNRAS, 458, 2024
Tarnopolski, M. 2016c, Ap&SS, 361, 125
Tsutsui, R., Yonetoku, D., Nakamura, T., Takahashi, K., & Morihara, Y. 2013, MNRAS, 431, 1398
Veres, P., Bagoly, Z., Horváth, I., Mészáros, A., & Balázs, L. G. 2010, ApJ, 725, 1955
von Kienlin, A., Meegan, C. A., Paciesas, W. S., et al. 2014, ApJS, 211, 13
Woosley, S. E. 1993, ApJ, 405, 273
Woosley, S. E., & Bloom, J. S. 2006, ARA&A, 44, 507
Yang, E. B., Zhang, Z. B., & Jiang, X. X. 2016, Ap&SS, 361, 257
Yonetoku, D., Murakami, T., Tsutsui, R., et al. 2010, PASJ, 62, 1495
Zhang, B., Zhang, B.-B., Virgili, F. J., et al. 2009, ApJ, 703, 1696
Zhang, B.-B., Zhang, B., Murase, K., Connaughton, V., & Briggs, M. S. 2014, ApJ, 787, 66
Zhang, Z.-B., & Choi, C.-S. 2008, A&A, 484, 293
Zhang, Z.-B., Yang, E.-B., Choi, C.-S., & Chang, H.-Y. 2016, MNRAS, 462, 3243
Zitouni, H., Guessoum, N., AlQassimi, K. M., & Alaryani, O. 2018, Ap&SS, 363, 223
Zitouni, H., Guessoum, N., Azzam, W. J., & Mochkovitch, R. 2015, Ap&SS, 357, 7